ARTICLE

Melting Mechanism and Structure Evolution of Au Nanofilms Explored by Molecular Dynamics Simulations

Guo-bing Zhou, Zhen Yang*, Fang-jia Fu, Na Hu, Xiang-shu Chen*, Duan-jian Tao

College of Chemistry and Chemical Engineering, Jiangxi Inorganic Membrane Materials Engineering Research Center, Jiangxi Normal University, Nanchang 330022, China

(Dated: Received on February 2, 2015; Accepted on May 28, 2015)

The melting mechanism and structure evolution of two-dimensional Au nanofilms with different thicknesses have been investigated in detail by using classical molecular dynamics simulations. The simulation results demonstrate that all Au nanofilms display a two-stage melting behavior of surface premelting and homogenous melting. Furthermore, the premelting behavior only occurs in the outermost layers but the other inner layers always keep a stable solid state until the corresponding melting point, which is different from the premelting behavior from surface into the interior in zero-dimensional Au nanocluster and one-dimensional Au nanowire. Meanwhile, the increase of nanofilm thickness can lead to an increase of melting point. During the premelting process, the surface reconstruction from the {100} plane to the {111} plane has directly been observed at a atomic level for all Au nanofilms. However even for the thinnest L2 nanofilm, the surface stress can't induce such surface reconstruction until temperature is up to 500 K, while similar surface reconstruction induced by surface stress can be observed at much lower temperature for the Au nanowire due to its higher surface-to-volume ratios compared to the Au nanofilm. In addition, our simulation results show that the thinnest Au nanofilm with two atomic layers can be broken into independent one-dimensional nanowires when the temperature reaches a certain value.

Key words: Phase transition, Surface reconstruction, Au nanofilm, Molecular dynamics simulation

I. INTRODUCTION

Understanding and predicting the properties of nanostructures is a significant and ongoing challenge within nanoscience and nanotechnology. In the past decades, gold-based nanostructures have received much attention due to their potential applications in heterogeneous catalysis, magnetic and microelectronic devices [1−8]. Exploring the structure-function relationship in nanostructures is necessary to require a comprehensive understanding of the phase and structure behavior of these systems. As the size of materials reduces to nanoscale, nevertheless, the fabrication and investigation of nanoscale materials are relatively tough to proceed in the available instruments and equipments. As a powerful analysis tool, molecular dynamics (MD) simulations can provide direct insights into the whole melting process of nanostructures at an atomic level. In past decades, considerable theoretical simulation studies [9−19] focused on their melting mechanism and structure evolution of zero- and one-dimensional Au nanostructures, finding that their enormous surface-to-volume ratios and structure characteristics can lead to different premelting behaviors prior to the homogenous melting. For the Au nanoclusters [9, 11], the most studies showed that their melting process starts from the surface and then proceeds inwards. In contrast, the melting of Au nanowires with the helical multiwalled cylindrical structure starts from the interior atoms instead of the surface atoms [17]. Furthermore, the core-solid/shell-liquid coexistence phenomena were found for the premelting process of Au-Pt nanoclusters with the core-shell orderings while their premelting nature with the random orderings corresponds to the dynamic coexistence melting [9, 10].

On the other hand, the one-dimensional nanowires often exhibit the deformation of their surface structure [20−32]. Such surface deformation can be induced by the combined effect of surface stress and surface energy, which generally correspond to the kinetic and energetic driving forces for the structural transformation of nanowires, respectively [33]. For example, the simulations proposed by Diao *et al.* have shown the surface-stress-induced phase transformation of Au nanowires with the square cross-sectional area less than 4 nm^2 [30]. This phase transformation is from the face-centred-cubic (FCC) structure into the body-centered-tetragonal (BCT) structure along with the change of

*Authors to whom correspondence should be addressed. E-mail: yangzhen@jxnu.edu.cn, cxs66cn@jxnu.edu.cn

{100} plane to {110} plane. On one hand, such spontaneous transformation can be attributed to that the compressive stress-strain inside the nanowires with {100} plane can be induced by the tensile surface-stress components along the axial direction [30]. On other hand, the surface energy of the BCT nanowire with {110} plane is also lower than that of the FCC nanowire with {100} plane, which is energetically favorable for the phase transformation [30]. Interestingly, similar FCC-BCT phase transformations have been observed experimentally by using *in situ* high-resolution transmission electron microscopy (HRTEM) [34]. In addition, adjusting temperature and pressure conditions can also result in the phase transformations of nanowires [29, 30, 33, 35]. The thermal vibrations arising from an elevated temperature can help the surface stress to overcome the energy barriers between the FCC and BCT phases so that the Au nanowires with the square cross-sectional area even more than 4 nm^2 also present identical phase transformations [29, 30]. Alternatively, Delogu has demonstrated that the increasing hydrostatic pressure can increase the minimum cross-sectional area of Ag nanorods that allows a spontaneous FCC-BCT transformation [35]. Meanwhile, the removal of pressure can also lead to the inverse transformation from the BCT to FCC phases. Up to now, these previous studies have made great progress in controlling the thermodynamic properties of zero- and one-dimensional nanostructures, which is of importance on the design and preparation of nanostructures and their applications.

For two-dimensional metal nanofilms, most of recent studies mainly focused on their electrical and mechanical properties [36−39]. However, only relatively limited studies [40−43] have been carried out for the melting behavior and structure evolution of two-dimensional metal nanostructures, which may be distinctly different from nanocluters and nanowires. For example, earlier experiments [40] have firstly reported the thickness-induced the structural phase transformation of Au nanofilm from the {100} plane to the {111} plane and the critical thickness for this transition was found to be 8 atomic layers. The driving force for such structural transition was found to be a decrease of energy differences between the interfacial and boundary energies. Subsequently, the MD simulations of Hasmy and Medina [41] have well reproduced the above phase transformation process, suggesting that analogous surface transformations don't occur only for 5d transition metals but also for other FCC metals. Furthermore, they found that the activation energy for such transformation is significantly dependent on metal species and the critical thickness is closely related to the surface area [41]. Recent MD simulations by Yang and Wu [42] have revealed that the premelting-melting transition of Nb nanofilm only occurs when the thickness of the quasi-liquid film reduces down to 1.3 nm, *i.e.* the thickness of around 8 atomic layers. Despite enormous efforts, several important issues remain unresolved regarding the microscopic melting mechanism and structural evolution even for the pure metal nanofilms.

In this work, a series of MD simulations with quantum Sutton-Chen potential (Q-SC) model [44] have been carried out to explore the melting mechanism and structure evolution of Au nanofilms with different thicknesses. We mainly pay attention to the thickness-dependent premelting behavior and structure reconstruction of the surface layers of Au nanofilms during the heating processes. Several indicators including caloric curve, atomic distribution function, and Lindemann index, have been introduced to comprehensively characterize the melting processes from the viewpoints of energy, structure, and dynamics, respectively.

II. MODEL AND SIMULATION DETAILS

Because of the delocalized electrons existing in the metal system, we should consider not only the repulsive interactions between the nucleus, but also the cohesive force resulting from the local electron density. In the present work, therefore, the interactions between Au atoms are characterized by the Q-SC potential [44], which contains quantum corrections and predicts better temperature dependent properties for the zero-point energy. According to the Q-SC potential, the total potential energy for an N-atoms system is expressed as

$$U = \varepsilon \sum_i \left[\frac{1}{2} \sum_{j \neq i} V(r_{ij}) - c\sqrt{\rho_i} \right] \tag{1}$$

where $V(r_{ij})$ is a pair potential to account for the repulsive interactions and ρ_i is the local electron density. They are given by

$$V(r_{ij}) = \left(\frac{a}{r_{ij}} \right)^n$$
$$\rho_i = \sum_{j \neq i} \left(\frac{a}{r_{ij}} \right)^m \tag{2}$$

where r_{ij} is the separation distance between atoms i and j, c is a positive dimensionless, ε is a parameter with the dimensions of energy, a is the lattice constant, and m and n are positive integers (n>m). These above parameters were obtained by fitting the experimental cohesive and lattice parameter. For the Au atoms, the parameters of Q-SC potential are as listed: m=8, n=11, ε=7.8052 meV, c=53.581, and a=4.0651 Å [19]. Based on Q-SC potential, the previous simulation proposed by Wen *et al.* [19] has revealed that the calculated melting point of bulk Au is 1380 K, which is close to the experimental value of T_m=1338 K.

Four different thicknesses (denoted as Ln, n=2, 3, 5, 6) were considered in this work, which were derived from a bulk FCC Au crystal. The periodic boundary conditions with minimum image convention were used

DOI:10.1063/1674-0068/28/cjcp1502011

in both x and y directions during MD simulations, as well as two free {100} surfaces in z direction. Each atomic layer contained 72 Au atoms and the initial box length of both x and y directions was set to 24.47 Å. The Nose-Hoover thermostat with coupling times of 0.1 ps and the the Berendsen algorithm with coupling time of 2.0 ps were employed to maintain the constant temperature and pressure conditions, respectively. Then the Newton's equations of motion were integrated using the velocity Verlet algorithm with a time step of 1 fs. For each Au nanofilm, MD simulations were performed in a series of temperature conditions ranging from 20 K to 1300 K with an increment of 20 K, and the initial configuration at each temperature was from the final configuration of previous temperature point. At each temperature, NPT MD (P=0 atm) simulation was first run 0.1 ns to relax the system. Then NVT MD simulation was run 0.5 ns for equilibration, and finally the next 2 ns were for the production collection stage. All MD simulations in this work are performed by using the modified Tinker 4.2 code [45], which has been successfully used to study the bimetallic nanoparticles (Au and Pt) in our previous work [9, 10].

III. RESULTS AND DISCUSSION

To investigate the variation of the potential energy with the temperature (*i.e.*, the caloric curves) of Au nanofilms, we have calculated the average potential energy per atom under each temperature $\overline{U}$, which can be defined as [18]:

$$\overline{U} = \frac{1}{N}\sum_{i=1}^{N} U_i \tag{3}$$

where U_i denotes the potential energy of the ith atom and N is the total number of atoms. As shown in Fig.1, we can see clearly that the average potential energy of Au nanofilms almost linearly increases with temperature at the front and back of caloric curves, corresponding to the solid and liquid states of Au nanofilms, respectively. Approaching to the melting transition, however, the caloric curves display some fluctuations deviated from the linear increase, suggesting the premelting behavior may exist for these Au nanofilms during the heating process. Similar common phenomena have been observed for zero-dimensional nanoclusters [9−11, 13, 15] and one-dimensional nanowires [19, 27, 46, 47] in the previous simulations. For the L2 nanofilm, however, the caloric curve exhibits a unique drop near the melting transition, which is obviously different from other nanofilms. Recently, Wen and co-workers [28] have observed the similar drop position of caloric curves for Ni nanowires, where the one-dimentional nanowire begins to break into zero-dimentional nanoclusters. Generally, the melting point of each Au nanofilm should be characterized at the sharp rise in each caloric curve. But for

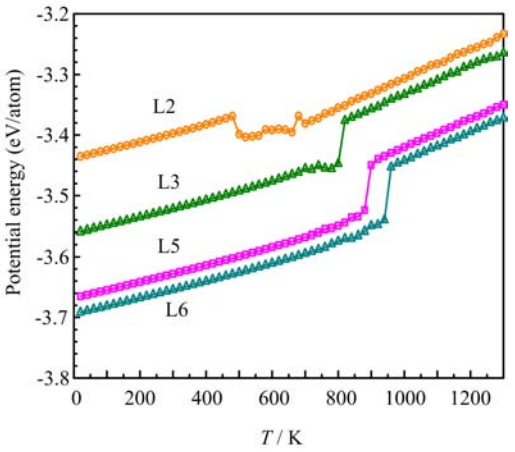

FIG. 1 The potential energy per atom as a function of temperature for the Au nanofilms with different thicknesses.

the L2 nanofilm, there is no obvious rise in the caloric curve. Its precise melting point will be determined from the following Lindemann index [48], which is more sensitive to the melting transition than the caloric curve.

The Lindemann index [48], *i.e.*, the root-mean-square bond length fluctuation, is also one of most effective and sensitive indicator to explore the melting process of nanostructures. To further provide a deep insight into the melting mechanism among different atomic layers of Au nanofilms, we present the variation of the Lindemann index of each layer as a function of the temperature in Fig.2. The Lindemann index of each layer $\delta_{\mathrm{L}(i)}$ is expressed as

$$\delta_{\mathrm{L}(i)} = \frac{2}{N_{\mathrm{L}(i)}(N_{\mathrm{L}(i)}-1)}\sum_{j<k}\frac{\sqrt{\langle r_{jk}^2\rangle - \langle r_{jk}\rangle^2}}{\langle r_{jk}\rangle} \tag{4}$$

where $N_{\mathrm{L}(i)}$ is the number of atoms of the ith layer, r_{jk} is the separation distance between atom j and k. Because the interlayer diffusion can result in the Au atoms deviating from the original position during the heating process of Au nanofilms, each Lindemann index doesn't actually stand for the corresponding atomic layer especially after the premelting behavior. In this way, however, it is still convenient to capture initial stage of the premelting behavior and surface isomerization for each atomic layer. As shown in Fig.2(d), the layer (1) and layer (6) indexes of L6 nanofilm, *i.e.* two surface layers, display an obvious and nonlinear increase at 800 K due to the separation of surface atoms from their lattice position induced by the strong thermal vibration. Upon further heating, all indexes show an enormously sharp jump at the corresponding melting point. After the homogeneous melting transition, the Lindemann index of each layer rises up to a large overall value (δ>0.20) with the increase of temperature, corresponding to the free movement of Au atoms in liquid state. However, we can also find from Fig.2(d) that the indexes of other

DOI:10.1063/1674-0068/28/cjcp1502011

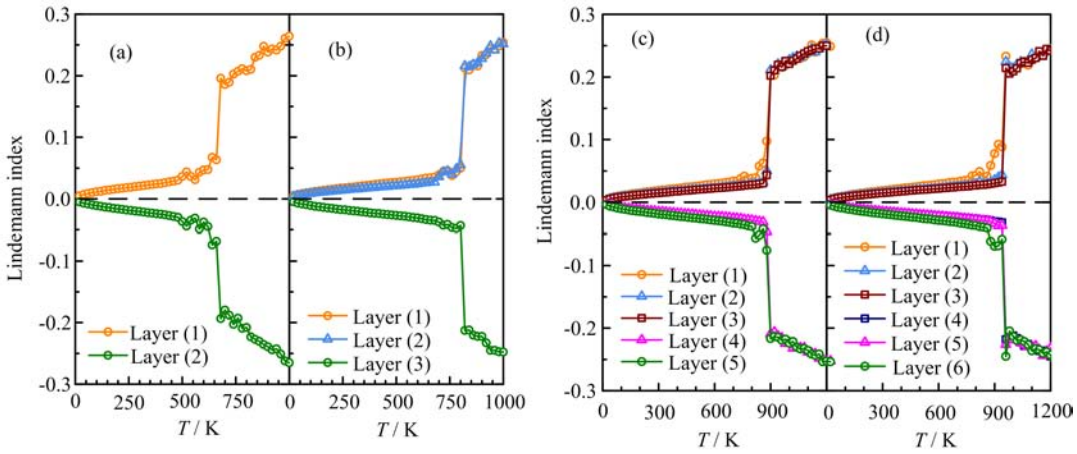

FIG. 2 The Lindemann index of each atomic layer as a function of temperature for the Au nanofilms with different thicknesses: (a) L2, (b) L3, (c) L5, and (d) L6 nanofilms.

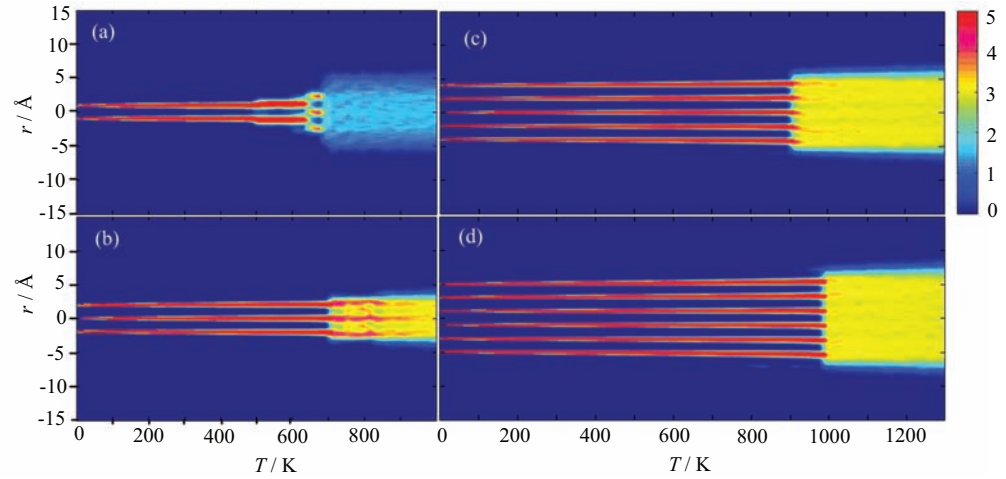

FIG. 3 The atomic number distribution perpendicular to the surface as a function of temperature for the Au nanofilms with different thicknesses: (a) L2, (b) L3, (c) L5, and (d) L6 nanofilms.

four inner layers are nearly linear growth with temperature until the complete melting occurs, indicating that the Au atoms of inner layers almost keep a solid state prior to the melting point. These features suggest that the premelting phenomenon only occurs in the outermost layers of L6 nanofilm, since the surface atoms have fewer nearest neighbors and more weakly bound compared to the inner atoms so that the surface atoms are very easy to diffuse and become liquid-like. Similar premelting behavior can be also found for L5 nanofilm, as shown in Fig.2(c). However, such premelting behavior of Au nanofilm is different from the premelting behavior from surface into the interior in the Au nanocluster [9] and nanowire [19]. Based on the caloric curve and Lindemann index, the melting points of Au nanofilms can be clearly characterized, which are 670±10 K (L2), 810±10 K (L3), 890±10 K (L5), 950±10 K (L6), respectively. Namely, the melting points of nanofilms increase monotonously with the thickness. It should be noted that the melting points of Au nanofilms are expected to be much lower than both the theoretical [19] and experimental [49] bulk values of Au crystal.

Apart from the energy viewpoint of caloric curve and Lindemann index, we also monitor the structure indicator to characterize the melting behavior of Au nanofilms, *i.e.* the variation of atomic number distribution along z direction (perpendicular to the nanofilm surfaces) with temperature. As shown in Fig.3, all atomic distribution functions show a certain number of parallel and separated color bands when the temperature is much lower than the corresponding melting point, indicating each atomic layer of Au nanofilms can be retained without interlayer diffusion far below the melting point. As the homogenous melting transition occurs, the ordered distribution is abruptly destroyed. But for the L2 nanofilm (see Fig.3(a)), there are four different stages of atomic distribution function during the heating process. The first stage is that the atomic

DOI:10.1063/1674-0068/28/cjcp1502011

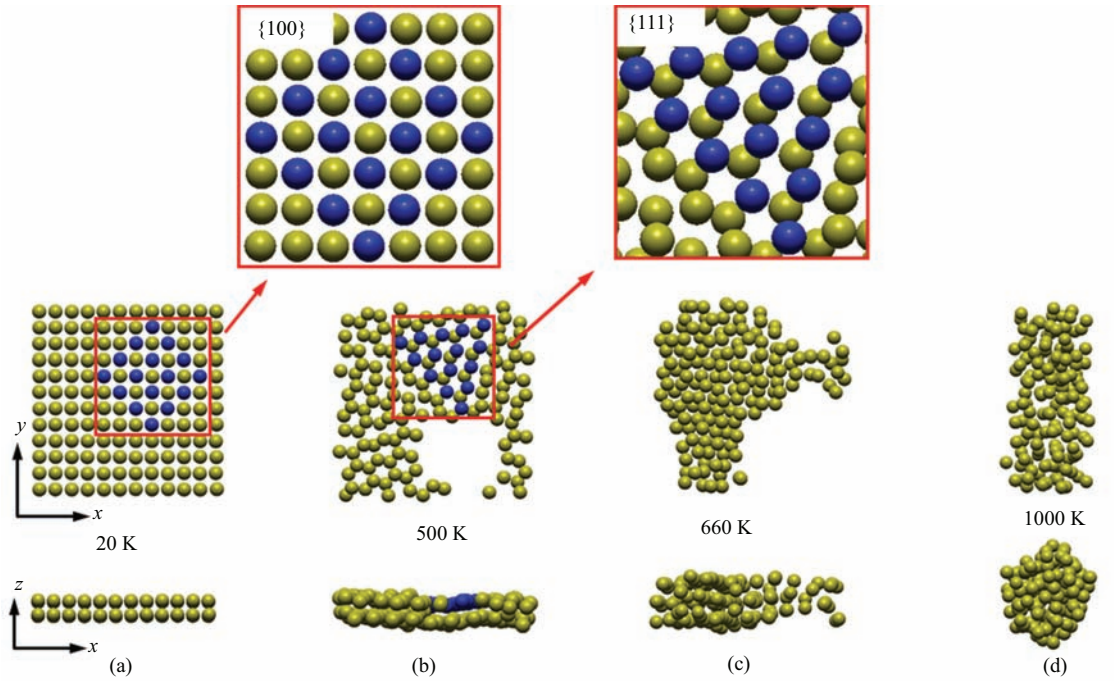

FIG. 4 The final configurations of L2 nanofilm at four typical temperatures. (a) 20 K, (b) 500 K, (c) 660 K, and (d) 1000 K. The blue spheres represent the Au atoms in the outermost layer.

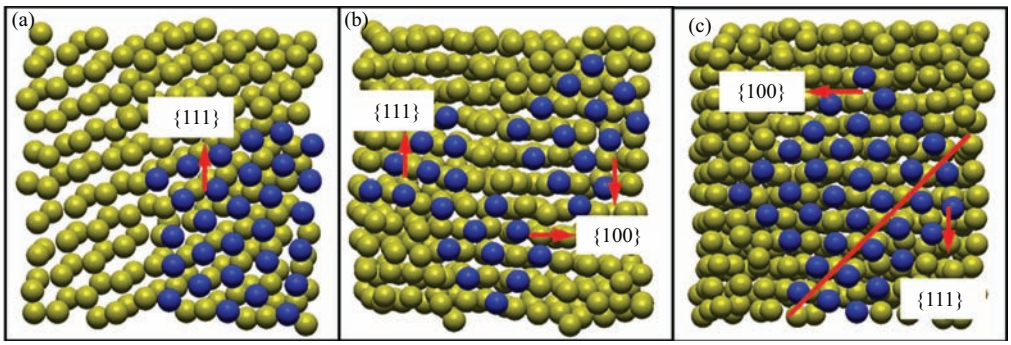

FIG. 5 The final configurations of (a) L3 nanofilm at 800 K, (b) L5 nanofilm at 880 K, and (c) L6 nanofilm at 940 K. The blue spheres represent the Au atoms in the outermost layer.

distribution function keeps two parallel and separated color bands from 0 K to 490 K. Then the second stage is that the color bands broaden obviously in the temperature range of 490 K to 630 K, suggesting the surface premelting behavior emerges. The third stage is that the two broadening bands are further divided into three color bands from 630 K to 690 K, corresponding to the formation of three atomic layers in the L2 nanofilm. Such premelting behavior may originate from that the L2 nanofilm only with surface atoms has the highest surface energy compared to other nanofilms so that the surface atoms have a strong trend to migrate inside nanofilm, which is favorable to reduce the surface energy [17−19]. This can be accepted as the reason for a unique drop in the caloric curve of L2 nanofilm, as shown in Fig.1. The final stage is that the three color bands merge into one large band when the temperature is up to 690 K. Furthermore, the final band width of L2 nanofilm is even bigger than that in the L3 nanofilm, suggesting that a unique structure evolution occurs for the L2 nanofilm. Subsequently, we can see only from the L2 snapshots of our simulation trajectories that the two-dimensional Au nanofilm can break into one-dimensional Au nanowire during the heating process, as shown in Fig.4. Additionally for the L3 nanofilm, we find that there is an obvious and lasting interlayer diffusion process prior to 810 K (see Fig.3(b)), corresponding to the premelting process.

In order to analyze the structure evolution processes of Au nanofilms intuitively, we present several final snapshots extracted from the trajectories of L2 nanofilm at a series of typical temperatures in Fig.4. At low tem-

DOI:10.1063/1674-0068/28/cjcp1502011

peratures, the atoms can only weakly vibrate around their equilibrium position, corresponding to that the initial shape and structure of L2 nanofilm is preserved before the premelting. As the temperature increases up to 500 K, the surface atoms of L2 nanofilm start to deviate from the equilibrium positions and undergo interlayer diffusion associating with the formation of a "hole", as shown in Fig.4(b). Such structure variation leads to the caloric curve of L2 nanofilm experiencing a sharp drop, as depicted the Fig.1. With further heating, the above "hole" gradually disappears and the neck shape is firstly found to be formed in L2 nanofilm at 660 K due to the movement of the unrestricted surface atoms, accompanying with the original two atomic layers divided into three irregular layers. This is consistent with the atomic distribution function of L2 nanofilm in Fig.3(a). As the temperature rises higher, we can unexpectedly see the formation of independent nanowires after the breaking of neck, which is analogous with the formation of nanoclusters during the melting process of nanowires [18, 19, 28]. As shown in Fig.4(d), the Au nanofilm almost completely transfers into independent nanowires with cylindrical structure when the simulation temperature increases up to 1000 K.

As shown in Fig.4 and Fig.5, we can see clearly that there exists the surface reconstruction of Au nanofilms from the {100} plane to the {111} plane when the temperature increases up to a certain value. Such surface reconstruction should be mainly determined by the surface energy differences between crystal planes and the mismatch between topmost layers and subsurface layers [50]. When the surface of Au nanofilm is from the {100} plane to the {111} plane, the decrease of surface energy is favorable for such surface reconstruction [29, 30, 51−53]. On the contrary, the surface reconstruction will lead to the mismatch between the {111} plane (*i.e.* the top layer) and the {100} plane (*i.e.* the subsurface layer), which is unfavorable for the reconstruction [40, 41, 50]. Besides the energetic factors, the kinetic factor, *i.e.* surface stress, also plays an important role in the surface reconstruction [20]. Compared to the one-dimensional nanowires, the two-dimensional nanofilms often exhibit lower surface-to-volume ratio so that the surface stress of nanofilms alone can't overcome the energy barriers at low temperatures. Only when the temperature increases up to a higher value, the strong thermal vibrations can help the surface stress to induce the surface reconstruction from the {100} plane to the {111} plane. For example, we can see from Fig.4 (a) and (b), even for the thinnest L2 nanofilm, its surface {100} planes can be always stable until temperature is up to 500 K, while similar surface reconstruction induced by the surface stress can be observed only at 100 K for the Au nanowire (its cross-sectional area is 1.83 nm×1.83 nm [30]. Apart from the L2 nanofilm, similar surface reconstruction has also been observed for other nanofilms at higher temperatures (>500 K).

IV. CONCLUSION

In this work, we have investigated the melting mechanism and structure evolution of Au nanofilms with different thicknesses by using classical MD simulations based on the quantum Sutton-Chen potential. The relevant melting mechanism has been characterized in detail by the combination of the caloric curve, atomic distribution function, and Lindemann index. Our simulation results demonstrated that the increase of thickness can lead to an increase of the melting temperature. Meanwhile, the premelting behavior of Au nanofilms only occurs in the outermost layers while other inner layers can be always stable until the melting point, which is different from the premelting behavior from surface into the interior in the Au nanocluster [9] and nanowire [19]. On the other hand, it is well-known that the surface energy of {111} plane is much lower than that of {100} plane, so that the surface reconstruction from the {100} plane to the {111} plane of all Au nanofilms can be observed due to the decrease of surface energy. However, the surface stress of nanofilms alone can't overcome the energy barriers of surface reconstruction at low temperatures. Even for the thinnest L2 nanofilm, its surface {100} planes can be always stable until temperature is up to 500 K, while similar surface reconstruction induced by the surface stress can be observed at much lower temperatures for the Au nanowire [30]. This is because the two-dimensional nanofilms have lower surface-to-volume ratios than those of one-dimensional nanowires. In addition, the simulations showed for the first time that the thinnest L2 nanofilm is broken into two independent nanowires during the melting process. Our simulation results are helpful for experimental scientists to understand the thermal stability and structure evolution of Au nanofilms at an atomic level, which is very important for the preparation and application of two-dimensional nanostructures.

V. ACKNOWLEDGMENTS

This work was supported by the National Natural Science Foundation of China (No.21306070 and No.21463011), the National High Technology Research and Development Program of China (No.2012AA03A609), Key Technology R&D Program of Jiangxi Province (No.20114ACB01200), and Science and Technology Project of Universities in Jiangxi Province (No.KJLD12005).

[1] A. Corma and P. Serna, Science **313**, 332 (2006).
[2] A. T. Bell, Science **299**, 1688 (2003).
[3] G. A. Hutchings, Nat. Chem. **1**, 584 (2009).
[4] D. Ho, X. L. Sun, and S. H. Sun, Acc. Chem. Res. **44**, 875 (2011).

DOI:10.1063/1674-0068/28/cjcp1502011

[5] F. Xiao, F. Patolsky, E. Katz, J. F. Hainfeld, and I. Wilner, Science **299**, 1877 (2003).
[6] Q. G. Zhang, B. Y. Cao, X. Zhang, M. Fujii, and M. Takahashi, Phys. Rev. B **74**, 134109 (2006).
[7] R. A. Hatton, M. R. Willis, and M. A. Chesters, J. Mater. Chem. **13**, 722 (2003).
[8] V. Rodrigues, T. Fuher, and D. Ugarte, Phys. Rev. Lett. **85**, 4124 (2000).
[9] Z. Yang, X. N. Yang, and Z. J. Xu, J. Phys. Chem. C **112**, 4937 (2008).
[10] Z. Yang, X. N. Yang, Z. J. Xu, and S. Y. Liu, Phys. Chem. Chem. Phys. **11**, 6249 (2009).
[11] R. Huang, Y. H. Wen, G. F. Shao, and S. G. Sun, J. Phys. Chem. C **117**, 4278 (2013).
[12] Y. T. Wang and S. Teitel, J. Chem. Phys. **122**, 214722 (2005).
[13] J. H. Shim, B. J. Lee, and Y. W. Cho, Surf. Sci. **512**, 262 (2002).
[14] C. L. Cleveland, W. D. Luedtke, and U. Landman, Phys. Rev. Lett. **81**, 2036 (1998).
[15] N. Y. Wang, S. I. Rokhlin, and D. F. Farson, Nanotechnology **19**, 415701 (2008).
[16] R. Ferrando, J. Jellinek, and R. L. Johnston, Chem. Rev. **108**, 845 (2008).
[17] J. L. Wang, X. S. Chen, G. H. Wang, B. L. Wang, W. Lu, and J. Zhao, Phys. Rev. B **66**, 085408 (2002).
[18] Y. Zhang, Y. H. Wen, J. C. Zheng, and Z. Z. Zhu, Phys. Lett. A **373**, 3454 (2009).
[19] Y. H. Wen, Y. Zhang, J. C. Zheng, Z. Z. Zhu, and S. G. Sun, J. Phys. Chem. C **113**, 20611 (2009).
[20] F. Ma, K. W. Xu, and P. K. Chu, Mater. Sci. Eng. R **74**, 173 (2013).
[21] E. Z. Silva, A. J. R. Silva, and A. Fazzio, Phys. Rev. Lett. **87**, 256102 (2001).
[22] J. S. Lin, S. P. Ju, and W. J. Lee, Phys. Rev. B **72**, 085448 (2005).
[23] B. L. Wang, J. L. Wang, and G. H. Wang, J. Chem. Phys. **120**, 3431 (2004).
[24] J. J. Lao and D. Moldovan, Appl. Phys. Lett. **93**, 093108 (2008).
[25] S. K. R. S. Sankaranarayanan, V. R. Bhethanabotla, and B. Joseph, J. Phys. Chem. C **111**, 2430 (2007).
[26] M. I. Haftel and K. Gall, Phys. Rev. B **74**, 035420 (2006).
[27] G. Ouyang, G. W. Yang, and G. H. Zhou, Nanoscale **4**, 2748 (2012).
[28] Y. H. Wen, Z. Z. Zhu, R. Z. Zhu, and G. F. Shao, Phys. E **25**, 47 (2004).
[29] J. K. Diao, K. Gall, and M. L. Dunn, Phys. Rev. B **70**, 075413 (2004).
[30] J. K. Diao, K. Gall, and M. L. Dunn, Nat. Mater. **2**, 656 (2003).
[31] K. Gall, J. K. Diao, M. L. Dunn, M. Haftel, N. Bernstein, and M. J. Mehl, J. Eng. Mater. Technol. **127**, 417 (2005).
[32] M. Konuk and S. Durukanoglu, Nanotechnology **23**, 245707 (2012).
[33] F. Ma and K. W. Xu, Appl. Surf. Sci. **254**, 4415 (2008).
[34] H. Zheng, A. J. Cao, C. R. Weinberger, J. Y. Huang, K. Du, J. B. Wang, Y. Y. Ma, Y. N. Xia, and S. X. Mao, Nat. Commun. **1**, 1 (2010).
[35] F. Delogu, J. Phys. Chem. C **114**, 3364 (2010).
[36] X. Zhang, H. Q. Xie, M. Fujii, H. Ago, K. Takahashi, T. Ikuta, H. Abe, and T. Shimizu, Appl. Phys. Lett. **86**, 171912 (2005).
[37] Y. Gan and J. K. Chen, Mech. Res. Commun. **36**, 838 (2009).
[38] Y. Gan and J. K. Chen, Appl. Phys. A **95**, 357 (2009).
[39] H. Lin, S. Xu, C. Li, H. Dong, and X. W. Wang, Nanoscale **5**, 4652 (2013).
[40] Y. Kondo, Q. Ru, and K. Takayanagi, Phys. Rev. Lett. **82**, 751 (1999).
[41] A. Hasmy and E. Medina, Phys. Rev. Lett. **88**, 096103 (2002).
[42] X. Y. Yang and D. Wu, Appl. Surf. Sci. **256**, 3197 (2010).
[43] R. Sankarasubramanian and K. Kumar, Comput. Mater. Sci. **49**, 386 (2010).
[44] Y. Qi, T. Cain, W. L. Johnson, and W. Goddard, J. Chem. Phys. **115**, 385 (2001).
[45] J. W. Ponder, *Tinker 4.2: Software Tools for Molecular Design*, Saint Louis, MO: Washington University School of Medicine, (2004).
[46] X. Y. Yang and X. J. Chen, Eur. Phys. J. D **66**, 128 (2012).
[47] X. Y. Yang, W. Y. Hu, F. S. Liu, and Y. Li, J. Phys. D **45**, 485304 (2012).
[48] S. Alavi and D. L. Thompson, J. Phys. Chem. A **110**, 1518 (110).
[49] C. Kittel, *Introduction to Solid State Physics*, New York: Wiley, (1996).
[50] V. Fiorentini, M. Methfessel, and M. Scheffler, Phys. Rev. Lett. **71**, 1051 (1993).
[51] W. Liang and M. Zhou, Phys. Rev. B **73**, 115409 (2006).
[52] Y. Shu, J. M. Zhang, K. W. Xu, and V. Ji, Solid State Commun. **141**, 384 (2007).
[53] M. I. Haftel and M. Rosen, Phys. Rev. B **64**, 195405 (2001).

DOI:10.1063/1674-0068/28/cjcp1502011